Journal of Applied Polymer Science

Fabrication of Graphene Supported Carbon-Coating Cobalt and Carbon Nanoshells for Adsorption of Toxic Gases and Smoke

Ningning Hong,[1] Lei Song,[1] Bibo Wang,[1] Bibe Yuan,[1] Yongqian Shi,[1] Yuan Hu[1,2]

[1]State Key Laboratory of Fire Science, University of Science and Technology of China, Hefei, Anhui 230026, People's Republic of China

[2]Suzhou Key Laboratory of Urban Public Safety, Suzhou Institute of University of Science and Technology of China, Suzhou, People's Republic of China

Correspondence to: Y. Hu (E-mail: yuanhu@ustc.edu.cn)

ABSTRACT: Graphene-supported carbon-coating cobalt and carbon nanoshells (Co/C-GNS and CNS-GNS) were fabricated and their applications in absorbing toxic gases and smoke have been investigated. Co_3O_4-loaded reduced graphite oxide was first prepared via a coprecipitation process, then carbon coatings on cobalt nanoparticles were fabricated by a catalytic carbonization process. The obtained hybrids were characterized by X-ray diffraction, transmission electron microscopy, Raman spectroscopy, N_2 absorption/desorption, and thermogravimetric analysis. Co/C core/shell structure and hollow carbon nanoshells in the size range of 15–22 nm were anchored onto the graphene surfaces. The resultant Co/C-GNS and CNS-GNS performed an important function in CO removal and smoke suppression during the combustion of acrylonitrile-butadiene-styrene. The good performance could be attributed to the combination effect of physical barrier of the GNS, porosity structure of the carbon nanoshells, and carbonization of the Co nanoparticles. © 2014 Wiley Periodicals, Inc. J. Appl. Polym. Sci. **2014**, *131*, 40457.

KEYWORDS: adsorption; applications; nanotubes; graphene and fullerenes; catalysts; degradation

Received 25 September 2013; accepted 16 January 2014
DOI: 10.1002/app.40457

INTRODUCTION

Graphene, a two-dimensional carbon, has been a rising star in material science since it was discovered in 2004.[1] Because of its astonishing properties, graphene shows potential applications in composites, energy-related systems, sensors, electronics, and photonic.[2–4] Among various methods for producing graphene, the chemical reduction of graphite oxide (GO) seems to be the most promising one for the large-scale production.[5,6] The existence of oxygen-containing groups and high specific surface area make graphene an excellent two-dimensional support to load nanoparticles for various applications.

Core/shell nanostructures have attracted intensive research interest due to their unique structures and properties. Metal or metal oxide nanoparticles have potential applications in many fields; however, they are easily to agglomerate and hard to resist the environmental oxidation and acid solution. Thus, coating nanoparticles with other materials seems to be an effective method. Compared with polymer and silica coatings, carbon shells, especially graphitic carbon have exhibited better thermal stability and satisfactory oxidation resistance.[7] Until now, carbon coating nanoparticles has been prepared by several methods, such as arc-discharge,[8] ion-beam sputtering,[9] chemical vapor deposition (CVD),[10,11] and catalytic carbonization.[12–14] The arc-discharge and ion-beam sputtering are usually processed under harsh synthetic conditions with low yield. CVD is widely used to prepare high-quality core/shell structure, nevertheless it is stuff wasting and requires high temperature. The catalytic carbonization, in which catalysts containing Fe, Ni or Co element and carbon source are carbonized at a certain temperature, is a promising route due to its simplicity, low cost, and easy availability. However, the yield obtained by this method still needs improvement.

Graphene-based nanostructures have been extensively reported because they could combine properties of individual component. Decorating graphene sheets with other components will prevent the aggregation of graphene sheets, and keep the large specific surface area of the hybrid, which is the prerequisite for adsorption, photocatalysis, and other fields.[15–18] The reduced graphene oxide (RGO) intercalated with Co_3O_4 was prepared through a hydrothermal method, and exhibited a high response to NO_2 and methanol at room temperature.[15] The experimental

result demonstrated that the CO_2 uptake capacity of the layered double hydroxide was increased using GO as a support.[16] Liu et al. fabricated magnetic Fe_3O_4/carbon-graphene hybrids with hierarchical nanostructures via a hydrothermal process by using glucose as a carbon source. The rapid and efficient adsorption of organic dyes from water was obtained by the hybrids.[17] Zhao et al. reported a method for preparing three-dimensional carbon-based architectures consisting of mesoporous carbon spheres intercalated between graphene sheets, which showed a substantially high power capability.[18]

In this work, a new strategy was reported for fabricating graphene supported carbon coating cobalt nanoparticle (Co/C-GNS) hybrids. First, Co_3O_4 loaded RGO was prepared via a facile process by coprecipitation of Co^{2+} in the presence of GO. Then Co-C/GNS was prepared by a catalytic carbonization process using polypropylene (PP)/organically modified montmorillonite (OMMT) as a carbon source. The as-prepared Co/C-GNS demonstrated good performance in CO removal and smoke suppression during the combustion of acrylonitrile-butadiene-styrene (ABS).

EXPERIMENTAL

Materials

Nature graphite, $Co(NO_3)_2$•$6H_2O$, NaOH and tetrahydrofuran (THF) were purchased from Sinopharm Chemical Reagent (Shanghai, China). Hydrofluoric acid (HF) and H_2SO_4 were bought from Guangfu Fine Chemial Research Institute (Tianjin, China). PP (F401, homopolymer) was supplied as pellets by Yangzi Petrochemical (Jiangsu, China). Maleic anhydrate grafted polypropylene (MAPP, 1.0–2.0 MA%) and OMMT were kindly provided by Keyan company (Anhui, China). ABS (747S) was supplied as pellets by Jurong Chemical (Guangdong, China).

Preparation of Co/C-GNS and CNS-GNS

The recipe described herein is based on the experimental result of previous report.[14] GO was prepared by oxidation of nature graphite according to Hummers' method.[19] $Co(NO_3)_2$•$6H_2O$ was dispersed to the GO suspension by sonication to form a stable solution. The mixture was adjusted to a pH value of 10.5 by dripping NaOH solution, and then heated to 120°C for 5 h. The precursor Co_3O_4-RGO was collected by centrifuging and washing before drying. The Co_3O_4-RGO was melt-mixed with PP, MAPP, and OMMT in a twin-roller mill at 175°C for 15 min. After that the mixed composite was inserted in a quartz tube, which was maintained at 700°C for a certain time with the protection of inert atmosphere. The Co/C-GNS was obtained by dissolving raw powders in HF solution for 12 h. The further treatment of Co/C-GNS in H_2SO_4 solution resulted in the formation of CNS/GNS.

Characterization

X-ray diffraction (XRD) patterns were performed with a Japan Rigaku D/Max-Ra rotating anode X-ray diffractometer equipped with a Cu-Ka tube and Ni filter ($\lambda = 0.1542$ nm).

Transmission electron microscopy (TEM) micrographs were obtained by JEOL 2010 with an acceleration voltage of 200 kV. Specimens for the high resolution electron microscopy (HRTEM) measurements were obtained by dripping sample suspension onto a lacy carbon film supported by Cu grids.

Raman spectroscopy measurements were carried out at room temperature with a SPEX-1403 laser Raman spectrometer (SPEX Co, USA) with excitation provided in back-scattering geometry by a 514.5 nm argon laser line.

The Brunauer-Emmett-Teller (BET) surface area and pore volume were measured by the nitrogen gas adsorptiondesorption method at 77 K using a TriStar II 3020 Micrometrics apparatus. The pore size distribution was calculated by the Barrett Jayner Halenda (BJH) method using the desorption branch of the isotherm.

The thermogravimetric analysis (TGA) was carried out on the TGA Q5000 IR thermogravimetric analyzer (TA instruments, USA) at a heating rate of 20°C/min in air atmosphere.

The combustion test was performed on the cone calorimeter (FTT, UK) test in accordance with ISO 5660 standard procedures with an external heat flux of 35 kW/m^2.

The smoke-generating tests were performed on the NBS smoke burner chamber according to ASTM Test Method E662. The specimens were exposed to non-flaming conditions, which was achieved using an electrically heated radiant energy source that produced an irradiance level of 25 kW/m^2.

RESULTS AND DISCUSSION

The synthetic routes for the Co/C-GNS and CNS/GNS hybrids are illustrated in Figure 1. First, nature graphite is oxidized to GO by Hummers' method, resulting in the introduction of abundant oxygen-containing groups (-OH, -COOH). The positive Co^{2+} are captured by the negatively charged oxygen-containing groups on the GO sheets via electrostatic interaction, and then Co_3O_4 nanoparticles are precipitated on GO in the presence of NaOH solution. Meanwhile, GO is *in situ* reduced to RGO during the coprecipitaion process. The Co_3O_4/RGO is then melt-blended with PP and OMMT to prepare the composite. According to previous reports, PP/OMMT nanocomposite could be good a carbon source for producing carbon nanomaterials with large quantity due to the proton acidic effect of OMMT layers.[14,20] The obtained composite is then carbonized at 700°C to prepare raw Co/C-GNS material. Herein, pyrolytic hydrocarbons from the decomposition of PP/OMMT deposit on the RGO supported Co_3O_4 nanoparticles, and the graphene supported Co/C core/shell nanostructures are eventually produced. After treated with HF, OMMT layers are removed, giving Co/C-GNS structure. The graphene supported hollow carbon nanoshells (CNS-GNS) are obtained by further treating Co/C-GNS with H_2SO_4.

The XRD patterns of the as-prepared samples are displayed in Figure 2. GO presents two characteristic diffraction peaks at around 11.5° and 43°, which are ascribed to the (002) and (111) reflections of GO. The interlayer spacing of (002) plane is calculated to be 0.88 nm due to the incorporation of oxygen-containing groups on the GO surface. The XRD pattern of Co_3O_4-RGO shows characteristic (111), (220), (311), (511), and (440) diffraction peaks, which are in accordance with the values

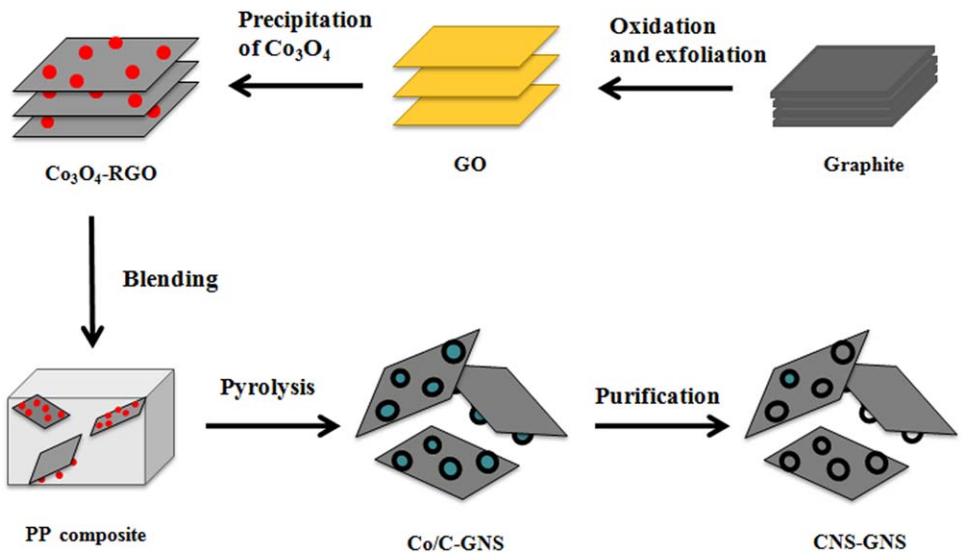

Figure 1. Schematic illustration of the synthesis routes for the Co/C-GNS and CNS-GNS hybrids. [Color figure can be viewed in the online issue, which is available at wileyonlinelibrary.com.]

of Co_3O_4 diffractions. No visible (002) diffraction of layered RGO is observed, implying the restacking of the graphene sheets is effectively prevented.[21] For the graphene, a broad peak around 24.9° is observed corresponding to the characteristic diffraction of graphitic carbon. This indicates graphene tends to conglomerate and reconstruct after the chemical reduction.[22] In the case of the Co/C-GNS, the strong diffraction peak at 26° corresponds to the formed graphitic carbon, and the strong peaks at 44.2° and 51.5° are assigned to (111) and (200) planes of metallic Co(0). This indicates that the supported Co_3O_4 is *in situ* reduced into Co(0) by the reductive hydrocarbons from PP decomposition.[14] After purification, the diffraction peak of graphitic structure becomes stronger while those corresponding to Co(0) turn weaker, indicating that metallic Co and other impurities have been almost removed.

The morphologies of the Co/C-RGO and CNS-GNS as well as GO, Co_3O_4-RGO, graphene are characterized by TEM as shown in Figure 3. GO presents transparent flake-like morphology with some areas closely packed. The sheets have lateral dimensions up to several micrometers [Figure 3(a)]. As shown in Figure 3(b), graphene is composed of crumpled and folded sheets with much smaller dimension. For the Co_3O_4-RGO, small Co_3O_4 nanoparticles with a size of ~16 nm are distributed densely on the surfaces of RGO nanosheets [Figure 3(c)]. Figure 3(d) shows a typical TEM image of the Co/C-GNS by using Co_3O_4-RGO as the catalyst precursor. Both core/shell structure and hollow carbon shells in the size range of 15–22 nm are anchored onto the graphene. HRTEM image of the Co/C-GNS [Figure 3(e)] further demonstrates the presence of core/shell (Co/C) nanostructure. The interlayer spacing of 0.2 nm is well corresponded to the value of Co(111) plane.[23] The crystalline plane of C(002) with a distance spacing of 0.37 nm can be clearly observed for the outer carbon nanoshells. The thickness of the carbon nanoshells falls in the range of 2–5 nm. In the TEM image of CNS-GNS, a large amount of hollow carbon nanoshells with a particle size of 18 nm are homogeneously attached on the graphene. The porous structure of CNS is derived from core/shell structures by removal of their cobalt cores.

Raman spectroscopy is used to characterize the graphitization degree of carbon materials, because it is sensitive to minor change inside the carbon layers. Figure 4 shows the Raman spectra of the Co/C-GNS and CNS-GNS with control of GO, Co_3O_4-RGO and graphene. All samples exhibit two prominent peaks located at around 1350 cm^{-1} and 1600 cm^{-1} in the Raman spectra. The former, called D band, originates from the defects or structural disorder, and the latter, named G band, is ascribed to the E_{2g} phonon of C sp^2 atoms.[24] The intensity ratio of D and G bands (I_D/I_G) is often used to estimate the disorder degree of graphitic materials. The I_D/I_G of graphene (1.65) is lower than that of GO (1.76) due to the recovery of sp^2 structure after reduction. For Raman spectrum of the Co_3O_4-RGO,

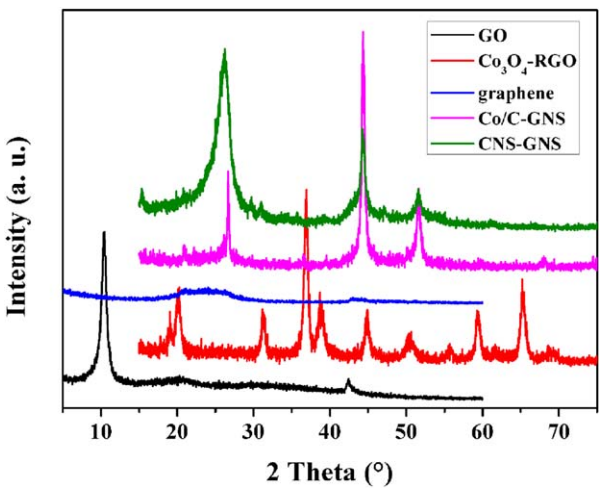

Figure 2. XRD patterns of GO, Co_3O_4-RGO, graphene, Co/C-GNS and CNS-GNS respectively. [Color figure can be viewed in the online issue, which is available at wileyonlinelibrary.com.]

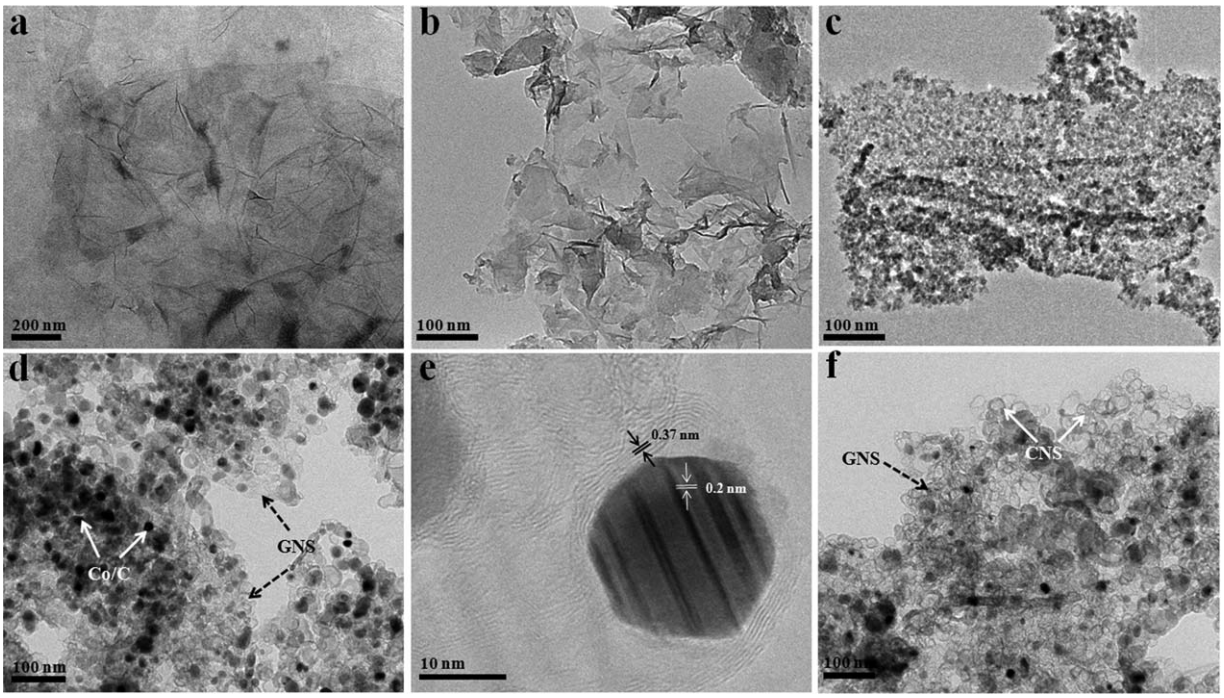

Figure 3. TEM images of GO (a), Co_3O_4-RGO (b), graphene (c), Co/C-GNS (d) and CNS-GNS (f) and HRTEM image of Co/C-GNS (e).

in addition to the D and G bands, Raman peaks at 491 and 596 cm^{-1} are attributed to the F2g mode of Co_3O_4, and those at 465 and 669 cm^{-1} correspond to the Eg and A1g modes of Co_3O_4, respectively.[21,25] Compared with GO, the I_D/I_G of Co_3O_4-RGO increases due to the decrease in the average size of the sp^2 graphtic domains after conjugating with Co_3O_4.[24] In the Raman spectra of Co/C-GNS, apart from the D and G bands, an additional peak at 687 cm^{-1} is well consistent with the typical Raman mode of metallic Co.[26] The I_D/I_G of Co/C-GNS is 1.55, which indicates the pyrolysis process promotes the formation of graphitic carbon (that is graphitic CNS). For CNS-GNS, the I_D/I_G is further decreased because impurities are removed after purification.

N_2 adsorption/desorption isotherms are employed to investigate the surface areas and porous structures of the graphene, Co/C-GNS and CNS-GNS, as shown in Figure 5. The isotherm of graphene belongs clearly to Type II almost without hysteresis, representing the characteristic of nonporous materials [Figure 5(a)].[27] Its BET specific surface area is only 53 m^2/g, probably due to the aggregation of graphene sheets. The isotherm of Co/C-GNS shows a little difference as compared with that of graphene and its BET specific surface area (530 m^2/g) is much higher. The BJH pore size distribution indicates that Co/C-GNS possesses a better porosity with a pore diameter of ~17 nm. The porosity mainly originates from the formation of secondary pores between CNS and GNS nanosheets.[28] At relatively low pressure, little gas is adsorbed on the surface of Co/C-GNS, but the adsorption increases largely at high pressure. Because of the storage of gas in the porous structure, a hysteresis loop occurs during the desorption period. The N_2 isotherm of CNS-GNS shows an evident hysteresis loop in the 0.4–0.9 range of relative pressure, representing a characteristic porous material. A steep fall of N_2 desorption is observed at P/P0 = 0.5, suggesting the characteristic of mesopore with narrow and slit-like shape.[18,29] The total pore diameter of CNS-GNS is 18 nm, which arises primarily from the formation of hollow CNS structures after removing inner Co cores.[18] From this sense, toxic gases are easily adsorbed in the hollow core of CNS, and the removal efficiency is related to the specific porous structure in the CNS-GNS material.

Figure 6 displays the photographs of THF solution of graphene, Co/C-GNS and CNS-GNS exposed to a magnetic field. As shown in Figure 6(a), graphene can be easily dispersed into THF to form dark suspension upon sonication. The external magnetic field has little effect on the solution. For the Co/C-GNS, dark stable suspension is formed after sonication. When

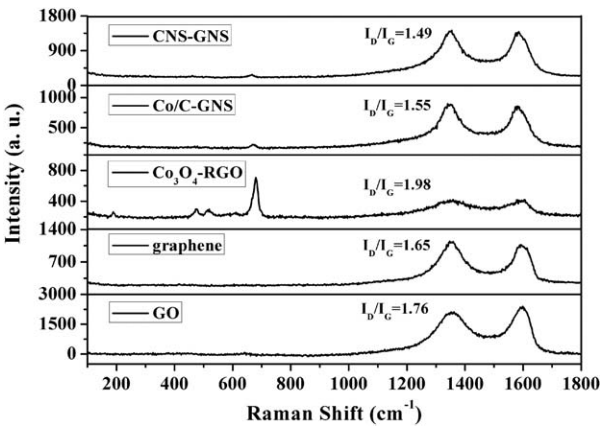

Figure 4. Raman spectra of GO, Co_3O_4-RGO, graphene, Co/C-GNS, and CNS-GNS, respectively.

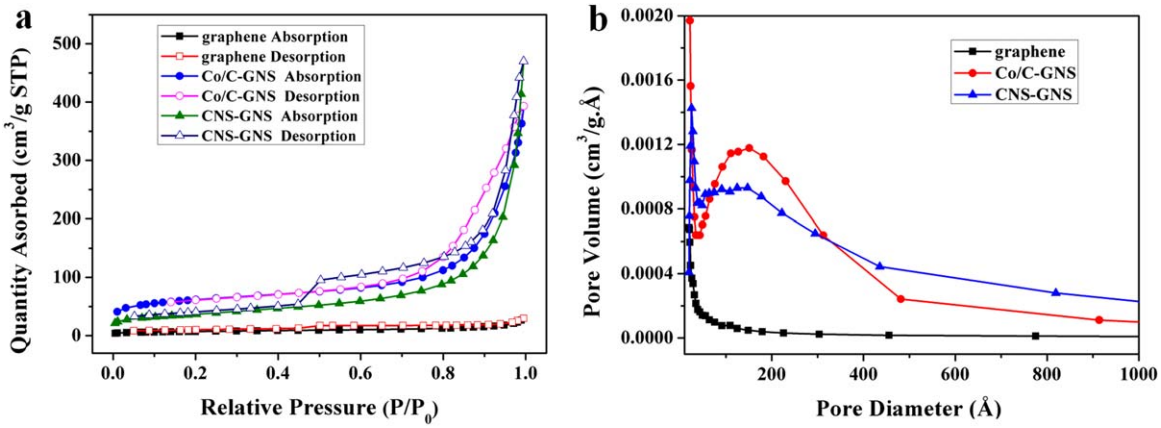

Figure 5. (a) Nitrogen adsorption-desorption isotherms and (b) pore size distribution curves of graphene, Co/C-GNS, and CNS-GNS. [Color figure can be viewed in the online issue, which is available at wileyonlinelibrary.com.]

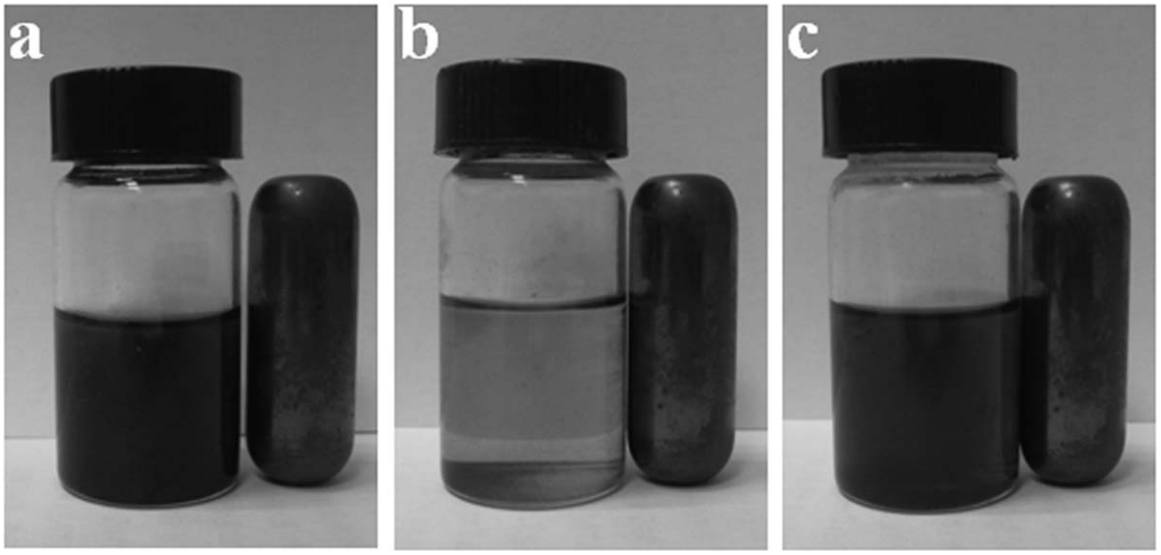

Figure 6. Photographs of graphene (a), Co/C-GNS (b), and CNS-GNS (c) dispersed into THF with a magnetic field.

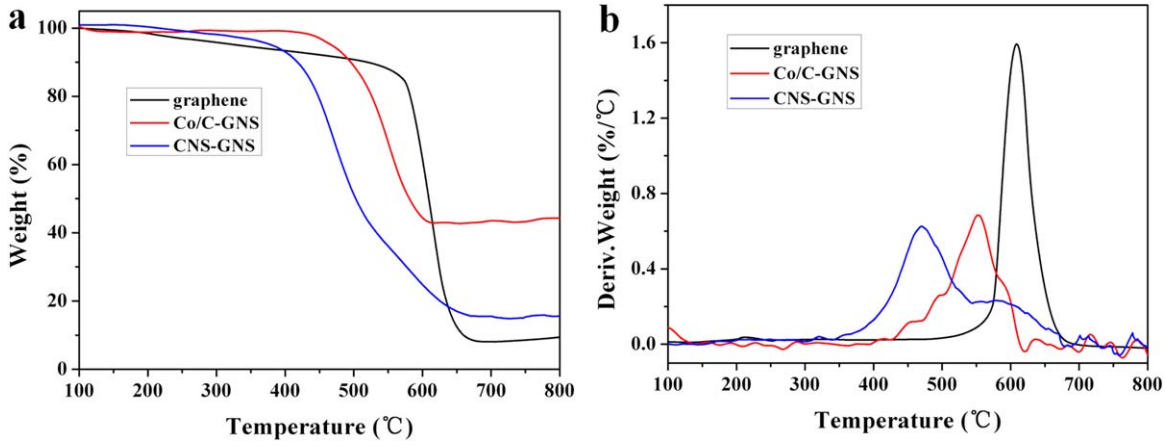

Figure 7. (a) TGA and (b) DTG curves for the graphene, Co/C-GNS, and CNS-GNS in air. [Color figure can be viewed in the online issue, which is available at wileyonlinelibrary.com.]

Table I. TGA Data for the Graphene, Co/C-GNS, and CNS-GNS in Air

Sample	$T_{5\%}$(°C)	T_{max}(°C)	Residue at 800 °C
Graphene	332	608.9	9.4%
Co/C-GNS	468	552.7	44.3%
CNS-GNS	381	470.0	15.6%

an external magnet is exposed, the Co/C-GNS can immediately be separated from the suspension [Figure 6(b)]. The response performance to magnetic field makes core/shell magnetic particles applied in many fields such as medicine and biology. CNS-GNS still remains in suspension with a magnet, indicating the formation of hollow CNS on GNS [Figure 6(c)].

The thermal behaviors of the graphene, Co/C-GNS and CNS-GNS are investigated by TGA (Figure 7) with the data listed in Table I. Graphene exhibits a slight weigh loss below 550°C which arises from the decomposition of remaining oxygen-containing groups. The remarkable weight loss between 550 and 700°C is attributed to the oxidation of the carbon skeleton of graphene.[30] The Co/C-GNS presents only one-step weight loss between 450 and 650°C, whose decomposition rate is much smaller than that of graphene. The high residual weight is associated with the inner Co nanoparticles in the Co/C-GNS hybrid. A significant mass drop of CNS-GNS around 460°C is due to the combustion of carbon skeleton. It is clear that the thermal stability of Co/C-GNS is much better than that of CNS-GNS.

As is well known, polymers belong to flammable materials with a great deal of heavy smoke and poisonous gases generating during combustion, which are the main reasons for the death in fires. The adsorption properties of the resultant hybrids towards CO are investigated by cone calorimeter, which is a powerful tool to predict the fire behavior of materials.[31] Figure 8 shows the variation of CO concentration with combustion time for ABS composites over Co/C-GNS and CNS-GNS. Pure ABS burns very fast with a high CO concentration of 0.55%. With the addition of graphene, the release of CO for the composite is obviously restrained. It is found that the CO cencentration decreases to ~0.40% over Co/C-GNS, with a reduction of 23.7% as compared to ABS. CNS-GNS exhibites high selectivity for CO adsorption (28.7%), which is higher than Co/C-GNS. Carbon nanotube (CNT) is widely used as a typical adsorbent for various gases due to its high specific surface area. The removal efficiency of CNT for CO could reach 31.5%, which is slightly higher than that of CNS-GNS. However, the time for maximum CO release occurs earlier for the composite containing CNT. From this sense, the Co/C-GNS and CNS-GNS not only have a high removal efficiency for CO, but also delay the time for CO release, which is related with their large surface area and porosity structures.[32]

Generally, the emission of smoke also plays a critical role in fire conditions. The variations of smoke density with combustion time over Co/C-GNS and CNS-GNS are plotted in Figure 9. The smoke density (SD) of ABS increases quickly to 559 Ds, reflecting the heavy smoke production in oxygen deficient environment. It is found that the SD values of composites treated with nanoparticles are all lower than that of pure ABS. Incorporating graphene plays little effect on reducing smoke release with a maximum of 529 Ds. As for the Co/C-GNS, the SD of the composite is largely decreased to 381 Ds, ~67.3% of that of pure ABS. It is found that the SD of ABS composite in the presence of CNS-GNS is quite low (471 Ds), indicating less smoke is evolved. CNT is another good adsorbent to adsorb the particulates released during combustion. It is clearly seen that the adsorption capability of CNT for smoke is very close to that of CNS-GNS. The unconspicious reduction in smoke production over graphene is mainly due to the barrier effect of graphene, while the porosity structure of CNS-GNS could largely absorb the smoke.[33,34] The largest reduction in smoke release is observed for Co/C-GNS, which is due to the combination effect of physical barrier of the GNS, porosity structure of the carbon nanoshells and catalytic carbonization of the Co cores.[7]

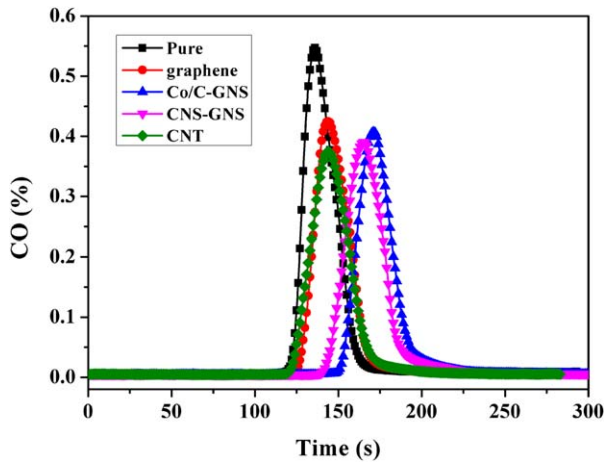

Figure 8. CO concentration versus time curves for ABS composites over graphene, Co/C-GNS, CNS-GNS, and CNT. [Color figure can be viewed in the online issue, which is available at wileyonlinelibrary.com.]

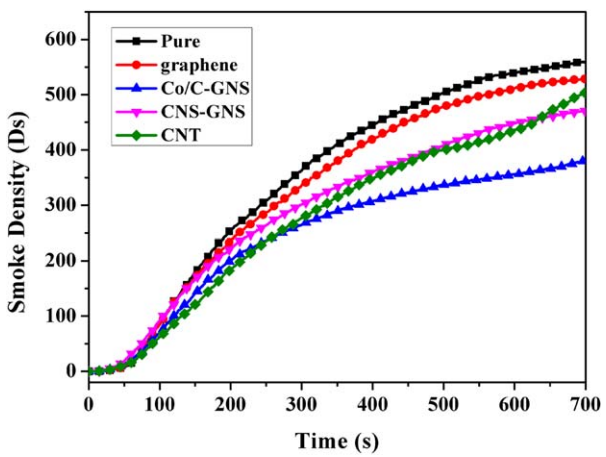

Figure 9. Smoke density versus time curves for ABS composites over graphene, Co/C-GNS, CNS-GNS, and CNT. [Color figure can be viewed in the online issue, which is available at wileyonlinelibrary.com.]

CONCLUSIONS

In summary, Co/C-GNS and CNS-GNS have been successfully prepared via a catalytic carbonization method. The hybridization of the graphene nanosheets and graphitic carbon nanoshells could significantly enhance the specific surface area and porosity. The resultant Co/C-GNS and CNS-GNS hybrids exhibit an extraordinary adsorption performance for toxic CO and heavy smoke during the combustion of ABS. Such adsorption is attributed to the combination effect of physical barrier of the GNS as well as porosity structure of the CNS, and carbonization of the Co nanoparticles. This work offers a facile and general approach to preparing graphene hybrids with porosity which may find their applications in the field of environment.

ACKNOWLEDGMENTS

The work was financially supported by the National Basic Research Program of China (973 Program) (No. 2012CB719701), the joint fund of Guangdong province and CAS (No.2010A090100017) and the Opening Project of State Key Laboratory of Fire Science of USTC (No. HZ2011-KF05).

REFERENCES

1. Novoselov, K. S.; Geim, A. K.; Morozov, S. V.; Jiang, D.; Zhang, Y.; Dubonos, S. V.; Grigorieva, I. V.; Firsov, A. A. *Science* **2004**, *306*, 666.
2. Huang, X.; Qi, X. Y.; Boey, F.; Zhang, H. *Chem. Soc. Rev.* **2012**, *41*, 666.
3. An, X. Q.; Yu, J. C. *RSC Adv.* **2011**, *1*, 1426.
4. Chen, X. M.; Wu, G. H.; Jiang, Y. Q.; Wang, Y. R.; Chen, X. *Analyst* **2011**, *136*, 4631.
5. Jiang, H. J. *Small* **2011**, *7*, 2413.
6. Eda, G.; Chhowalla, M. *Adv. Mater.* **2010**, *22*, 2392.
7. Kong, L. R.; Lu, X. F.; Bian, X. J.; Zhang, W. J.; Wang, C. *ACS Appl. Mater. Inter.* **2011**, *3*, 35.
8. Dravid, V. P.; Host, J. J.; Teng, M. H.; Elliot, B.; Hwang, J. H.; Johnson, D. L.; Mason, T. O.; Weertman, J. R. *Nature* **1995**, *374*, 602.
9. Babonneau, D.; Cabioc'h, T.; Naudon, A.; Girard, J. C.; Denanot, M. F. *Surf. Sci.* **1998**, *409*, 358.
10. Flahaut, E.; Agnoli, F.; Sloan, J.; O'Connor, C.; Green, M. L. H. *Chem. Mater.* **2002**, *14*, 2553.
11. Tian, F.; He, C. N. *Mater. Chem. Phys.* **2010**, *123*, 351.
12. Wang, B. L.; Tian, C. G.; Wang, L.; Wang, R. H.; Fu, H. G. *Nanotechnology* **2010**, *21*, 025606.
13. Lu, A. H.; Li, W. C.; Matoussevitch, N.; Spliethoff, B.; Bonnemann, H.; Schuth, F. *Chem. Commun.* **2005**, *1*, 98.
14. Chen, X. C.; Wang, H.; He, J. H. *Nanotechnology* **2008**, *19*, 325607.
15. Chen, N.; Li, X. G.; Wang, X. Y.; Yu, J.; Wang, J.; Tang, Z. A.; Akbar, S. A. *Sensor Actuat B-Chem* **2013**, *188*, 902.
16. Garcia-Gallastegui, A.; Iruretagoyena, D.; Gouvea, V.; Mokhtar, M.; Asiri, A. M.; Basahel, S. N.; Al-Thabaiti, S. A.; Alyoubi, A. O.; Chadwick, D.; Shaffer, M. S. P. *Chem. Mater.* **2012**, *24*, 4531.
17. Fan, W.; Gao, W.; Zhang, C.; Tjiu, W. W.; Pan, J. S.; Liu, T. X. *J. Mater. Chem.* **2012**, *22*, 25108.
18. Lei, Z. B.; Christov, N.; Zhao, X. S. *Energ. Environ. Sci.* **2011**, *4*, 1866.
19. Hummers, W. S.; Offeman, R. E. *J. Am. Chem. Soc.* **1958**, *80*, 1339.
20. Song, R. J.; Jiang, Z. W.; Bi, W. G.; Cheng, W. X.; Lu, J.; Huang, B. T.; Tang, T. *Chem-Eur. J.* **2007**, *13*, 3234.
21. Li, B. J.; Cao, H. Q.; Shao, J.; Li, G. Q.; Qu, M. Z.; Yin, G. *Inorg. Chem.* **2011**, *50*, 1628.
22. Dubin, S.; Gilje, S.; Wang, K.; Tung, V. C.; Cha, K.; Hall, A. S.; Farrar, J.; Varshneya, R.; Yang, Y.; Kaner, R. B. *ACS Nano* **2010**, *4*, 3845.
23. Zhang, F.; Hou, C. Y.; Zhang, Q. H.; Wang, H. Z.; Li, Y. G. *Mater. Chem. Phys.* **2012**, *135*, 826.
24. Xie, G. Q.; Xi, P. X.; Liu, H. Y.; Chen, F. J.; Huang, L.; Shi, Y. J.; Hou, F. P.; Zeng, Z. Z.; Shao, C. W.; Wang, J. *J. Mater. Chem.* **2012**, *22*, 25485.
25. Kim, H.; Seo, D. H.; Kim, S. W.; Kim, J.; Kang, K. *Carbon* **2011**, *49*, 326.
26. Arora, N.; Jagirdar, B. R. *J. Mater. Chem.* **2012**, *22*, 20671.
27. Freeman, J. J.; Gimblett, F. G. R.; Roberts, R. A.; Sing, K. S. W. *Carbon* **1987**, *25*, 559.
28. Li, B. J.; Cao, H. Q.; Shao, J.; Qu, M. Z. *Chem. Commun.* **2011**, *47*, 10374.
29. Su, J.; Cao, M. H.; Ren, L.; Hu, C. W. *J. Phys. Chem. C* **2011**, *115*, 14469.
30. Mei, X. G.; Ouyang, J. Y. *Carbon* **2011**, *49*, 5389.
31. Marney, D. C. O.; Russell, L. J.; Mann, R. *Fire Mater.* **2008**, *32*, 357.
32. Bandosz, T. J. *Catal. Today* **2012**, *186*, 20.
33. Mola, M.; Hallum, M.; Branton, P. *Adsorption* **2008**, *14*, 335.
34. Li, G. D.; Yu, H. X.; Xu, L. Q.; Ma, Q.; Chen, C.; Hao, Q.; Qian, Y. T. *Nanoscale* **2011**, *3*, 3251.